

# Cycle of phase, coherence and polarization singularities in Young's three-pinhole experiment

Xiaoyan Pang,<sup>1,\*</sup> Greg Gbur,<sup>2</sup> and Taco D. Visser<sup>1,3,4</sup>

<sup>1</sup>*School of Electronics and Information, Northwestern Polytechnical University, Xi'an, China*

<sup>2</sup>*Dept. of Physics and Optical Science, University of North Carolina at Charlotte, NC, USA*

<sup>3</sup>*Dept. of Physics and Astronomy, VU University, Amsterdam, The Netherlands*

<sup>4</sup>*EEMCS, Delft University of Technology, Delft, The Netherlands*

[\\*xytang@nwpu.edu.cn](mailto:xytang@nwpu.edu.cn)

**Abstract:** It is now well-established that a variety of singularities can be characterized and observed in optical wavefields. It is also known that these phase singularities, polarization singularities and coherence singularities are physically related, but the exact nature of their relationship is still somewhat unclear. We show how a Young-type three-pinhole interference experiment can be used to create a continuous cycle of transformations between classes of singularities, often accompanied by topological reactions in which different singularities are created and annihilated. This arrangement serves to clarify the relationships between the different singularity types, and provides a simple tool for further exploration.

© 2015 Optical Society of America

**OCIS codes:** (260.6042) Singular optics; (260.5430) Polarization; (260.2110) Electromagnetic optics; (030.1640) Coherence; (350.5030) Phase.

---

## References and links

1. M.S. Soskin and M.V. Vasnetsov, "Singular Optics," in: *Progress in Optics*, edited by E. Wolf (Elsevier, 2001), **42**, 219–276.
2. M.R. Dennis, K. O'Holleran and M.J. Padgett, "Singular optics: optical vortices and polarization singularities," in: *Progress in Optics*, edited by E. Wolf (Elsevier, 2001), **53**, 293–363.
3. J.F. Nye and M.V. Berry, "Dislocations in wave trains," *Proc. R. Soc. London* **336**, 165–190 (1970).
4. J.F. Nye, *Natural Focusing and Fine Structure of Light* (Institute of Physics, 1999).
5. M.V. Berry and M.R. Dennis, "Polarization singularities in isotropic random vector waves," *Proc. R. Soc. Lond. A* **457**, 141–155 (2001).
6. I. Freund, "Polarization singularity indices in Gaussian laser beams," *Opt. Commun.* **201**, 251–270 (2002).
7. I. Freund, "Polarization singularities in optical lattices," *Opt. Lett.* **29**, 875–877 (2004).
8. R.W. Schoonover and T.D. Visser, "Polarization singularities of focused, radially polarized fields," *Opt. Express* **14**, 5733–5745 (2006).
9. H.F. Schouten, G. Gbur, T.D. Visser and E. Wolf, "Phase singularities of the coherence functions in Young's interference pattern," *Opt. Lett.* **28**, 968–970 (2003).
10. G. Gbur and T.D. Visser, "Coherence vortices in partially coherent beams," *Opt. Commun.* **222**, 117–125 (2003).
11. D.G. Fischer and T.D. Visser, "Spatial correlation properties of focused partially coherent light," *J. Opt. Soc. Am. A* **21**, 2097–2102 (2004).
12. S.B. Raghunathan, H.F. Schouten and T.D. Visser, "Correlation singularities in partially coherent electromagnetic beams," *Opt. Lett.* **37**, 4179–4181 (2012).
13. S.B. Raghunathan, H.F. Schouten and T.D. Visser, "Topological reactions of correlation functions in partially coherent electromagnetic beams," *J. Opt. Soc. Am. A* **30**, 582–588 (2013).
14. G. Gbur, T.D. Visser and E. Wolf, "Hidden singularities in partially coherent and polychromatic wavefields," *Jnl. of Optics A* **6**, S239–S242 (2004).

15. G. Gbur and T.D. Visser, "Phase singularities and coherence vortices in linear optical systems," *Opt. Commun.* **259**, 428–435 (2006).
16. F. Flossmann, U.T. Schwarz, M. Maier, and M.R. Dennis, "Polarization singularities from unfolding an optical vortex through a birefringent crystal," *Phys. Rev. Lett.* **95**, 253901 (2005).
17. F. Flossmann, U.T. Schwarz, M. Maier, and M.R. Dennis, "Stokes parameters in the unfolding of an optical vortex through a birefringent crystal," *Opt. Express* **14**, 11402–11411 (2006).
18. I. Freund, "Poincaré vortices," *Opt. Lett.* **26**, 1996–1998 (2001).
19. T.D. Visser and R.W. Schoonover, "A cascade of singular field patterns in Young's interference experiment," *Opt. Commun.* **281**, 1–6 (2008).
20. M. Born and E. Wolf, *Principles of Optics*, 7<sup>th</sup> (expanded) ed. (Cambridge University Press, 1999).
21. C. Jönsson, "Elektroneninterferenzen an mehreren künstlich hergestellten Feinspalten," *Zeitschrift für Physik* **161**, 454–474 (1961). An English translation was published by D. Brandt and S. Hirschi, in the *American Journal of Physics* **42**, 4–11 (1974).
22. H.F. Schouten, N. Kuzmin, G. Dubois, T.D. Visser, G. Gbur, P.F.A. Alkemade, H. Blok, G.W. 't Hooft, D. Lenstra and E. Eliel, "Plasmon-assisted two-slit transmission: Young's experiment revisited," *Phys. Rev. Lett.* **94**, 053901 (2005).
23. F. Zernike, "The concept of degree of coherence and its applications to optical problems," *Physica* **5**, 785–795 (1938).
24. E. Wolf, "The influence of Young's interference experiment on the development of statistical optics," in *Progress in Optics*, E. Wolf (ed.), **50**, (Elsevier, 2007), 251–273.
25. R. Sawant, J. Samuel, A. Sinha, S. Sinha, and U. Sinha, "Nonclassical paths in quantum interference experiments," *Phys. Rev. Lett.* **113**, 120406 (2014).
26. G.C.G. Berkhout and M.W. Beijersbergen, "Method for probing the orbital angular momentum of optical vortices in electromagnetic waves from astronomical objects," *Phys. Rev. Lett.* **101**, 100801 (2008).
27. G.C.G. Berkhout and M.W. Beijersbergen, "Using a multipoint interferometer to measure the orbital angular momentum of light in astrophysics," *Jnl. of Optics* **11**, 094021 (2009).
28. G.C.G. Berkhout and M.W. Beijersbergen, "Measuring optical vortices in a speckle pattern using a multi-pinhole interferometer," *Opt. Express* **18**, 13836–13841 (2010).
29. R.W. Schoonover and T.D. Visser, "Creating polarization singularities with an N-pinhole interferometer" *Phys. Rev. A* **79**, 043809 (2009).
30. E. Wolf, *Introduction to the Theory of Coherence and Polarization of Light* (Cambridge University Press, 2007).
31. T. Setälä, J. Tervo, and A.T. Friberg, "Complete electromagnetic coherence in the space-frequency domain," *Opt. Lett.* **29**, pp. 328–330 (2004).
32. E. Wolf, "Coherence properties of partially polarized electromagnetic radiation," *Il Nuovo Cimento Ser. X* **13**, 1165–1181 (1959).
33. O. Korotkova, T.D. Visser and E. Wolf, "Polarization properties of stochastic electromagnetic beams," *Opt. Commun.* **281**, 515–520 (2008).
34. H.F. Schouten, T.D. Visser, D. Lenstra and H. Blok, "Light transmission through a sub-wavelength slit: waveguiding and optical vortices," *Phys. Rev. E*, **67**, 036608 (2003).
35. J.D. Jackson, *Classical Electrodynamics*, 3<sup>rd</sup> ed. (Wiley, 1999). See Sec. 7.2.
36. G.J. Gbur, *Mathematical Methods for Optical Physics and Engineering*, (Cambridge University Press, 2011). See Sec. 10.3.

## 1. Introduction

The discipline of singular optics [1,2], which is concerned with singularities in the topology of wavefields, has expanded dramatically over the past decade. It was originally concerned with singularities in the phase of scalar wavefields [3], lines in three-dimensional space where the amplitude of the field is zero and the phase is therefore undefined. Not long after, however, singularities of polarization were also described [4–8]. These are lines of circular polarization (C lines) on which the major axis of the polarization ellipse is undefined, and surfaces of linear polarization (L surfaces) on which the handedness of the polarization ellipse is undefined. In recent years, even more classes of singularities have been described. Singularities of the spectral degree of coherence (called correlation vortices or coherence vortices) have been found in partially coherent scalar wavefields, representing pairs of points where the field is completely uncorrelated [9–11]. Generalizing correlation singularities to electromagnetic fields, so-called eta singularities have been introduced [12, 13], which represent phase singularities of the electromagnetic correlation function.

It is less appreciated that these seemingly different classes of wave singularities are, in fact, closely related to each other. The connection between correlation singularities and phase singularities has been discussed in some detail [14, 15], and the connection between polarization singularities and phase singularities has also been investigated [16–18]. However, very little has been done to explore the full relationship between the different classes of singularities. It was shown in 2008, though, that it is possible to use Young’s double-slit experiment to create a cascade of singularities, in which changes in system parameters transform one class into another [19]. However, these singularities were not typical, or “generic”, because of the two-dimensional configuration in which they are created.

Young’s celebrated experiment, in which the light emanating from two pinholes or two slits is made to interfere on an observation screen [20], has played a pivotal role in the development of physical optics. The wave nature of light, and its transverse polarization properties were both established using Young’s setup. The experiment was also used to demonstrate the wave-particle duality of electrons [21]. In the field of plasmonics as well, basic experiments involve two-slit configurations [22]. Furthermore, the foundations of optical coherence theory, as developed by Zernike [23], stem from an analysis of Young’s experiment [24]. More recently, multi-pinhole interferometers have been used to various ends. For example, it has been suggested that they can be used to observe non-classical paths in quantum interference [25], to probe optical angular momentum and optical vortices [26–28], and to create polarization singularities [29].

In the present paper we introduce a special version of a Young three-pinhole interferometer and show how it can be used to create a continuous cycle of generic, singular field patterns on an observation screen. This is done by varying the polarization and coherence properties of light emerging from individual pinholes. In this cycle, a variety of different topological reactions between singularities occur. The cycle begins with an array of coherent phase singularities, from which polarization singularities, correlation singularities, and general electromagnetic correlation singularities are created via a change of the pinhole parameters. This arrangement highlights the relationship between the different classes of optical singularities and demonstrates a number of unusual effects.

## 2. Classes of optical singularities

A number of different classes of singularities have been discovered in optical fields; here we review the main features of the types to be encountered in the three-pinhole arrangement that we analyze. Phase singularities of the field component  $E_j$ , with  $j = x, y$ , occur at points where  $E_j(\mathbf{r}, \omega) = 0$ , and hence its phase is undefined. The topological charge  $s$  of such a singular point is defined as [4]

$$s = \frac{1}{2\pi} \oint_C d\phi, \quad (1)$$

where  $\phi$  is the phase of  $E_j$ , and the closed contour  $C$  that encloses the singularity is traversed in a counter-clockwise manner. Continuity of the wavefield  $E_j$  implies that the topological charge must have an integer value.

If the incident beam is random rather than deterministic, it has no definite field amplitude and phase and it must be described by a  $2 \times 2$  electric cross-spectral density matrix [30] that characterizes its state of coherence and polarization, namely

$$\mathbf{W}(\mathbf{r}_1, \mathbf{r}_2, \omega) = \begin{pmatrix} W_{xx}(\mathbf{r}_1, \mathbf{r}_2, \omega) & W_{xy}(\mathbf{r}_1, \mathbf{r}_2, \omega) \\ W_{yx}(\mathbf{r}_1, \mathbf{r}_2, \omega) & W_{yy}(\mathbf{r}_1, \mathbf{r}_2, \omega) \end{pmatrix}, \quad (2)$$

where

$$W_{ij}(\mathbf{r}_1, \mathbf{r}_2, \omega) = \langle E_i^*(\mathbf{r}_1, \omega) E_j(\mathbf{r}_2, \omega) \rangle, \quad (i, j = x, y). \quad (3)$$

Here  $E_i(\mathbf{r}, \omega)$  denotes a Cartesian component of the electric field of a typical realization of the statistical ensemble representing the beam. The angular brackets indicate an ensemble average. The spectral density is defined as

$$S(\mathbf{r}, \omega) = \langle |\mathbf{E}(\mathbf{r}, \omega)|^2 \rangle = \text{Tr} \mathbf{W}(\mathbf{r}, \mathbf{r}, \omega), \quad (4)$$

where Tr denotes the trace. The electromagnetic spectral degree of coherence  $\eta(\mathbf{r}_1, \mathbf{r}_2, \omega)$  of the field, which is a measure of the ability of the fields at points  $\mathbf{r}_1$  and  $\mathbf{r}_2$  to form interference fringes when brought together, is defined as [30]

$$\eta(\mathbf{r}_1, \mathbf{r}_2, \omega) = \frac{\text{Tr} \mathbf{W}(\mathbf{r}_1, \mathbf{r}_2, \omega)}{[\text{Tr} \mathbf{W}(\mathbf{r}_1, \mathbf{r}_1, \omega) \text{Tr} \mathbf{W}(\mathbf{r}_2, \mathbf{r}_2, \omega)]^{1/2}}. \quad (5)$$

For fully coherent fields this definition reduces to

$$\eta(\mathbf{r}_1, \mathbf{r}_2, \omega) = \frac{E_x^*(\mathbf{r}_1, \omega) E_x(\mathbf{r}_2, \omega) + E_y^*(\mathbf{r}_1, \omega) E_y(\mathbf{r}_2, \omega)}{|\mathbf{E}(\mathbf{r}_1, \omega)| |\mathbf{E}(\mathbf{r}_2, \omega)|}. \quad (6)$$

A coherence singularity occurs at pairs of points for which  $\eta(\mathbf{r}_1, \mathbf{r}_2, \omega) = 0$ , and consequently the phase of this correlation function is undefined. We note that such electromagnetic correlation singularities can occur even when the field is fully coherent. This happens when the two electric field vectors are orthogonal, i.e., when

$$\mathbf{E}^*(\mathbf{r}_1, \omega) \cdot \mathbf{E}(\mathbf{r}_2, \omega) = 0. \quad (7)$$

This observation leads to a relation between polarization singularities and electromagnetic coherence singularities. Eq. (7) is satisfied, for example, when the field at  $\mathbf{r}_1$  is linearly polarized along  $x$ , and the field at  $\mathbf{r}_2$  is linearly polarized along  $y$ . Both these points then lie on an L line (not necessarily the same L line), and at the same time also constitute an electromagnetic coherence singularity. We can therefore distinguish two types of electromagnetic coherence singularities: those that occur in fully coherent fields, and those that occur in partially coherent fields.

The existence of zeros of the function  $\eta$  even for fully coherent fields arises because this quantity represents the visibility of interference fringes produced in Young's experiment, and visibility can be affected by both the statistical similarity of the field at the pinholes and by their polarization. An alternative definition of the degree of coherence, that emphasizes statistical similarity, is given in [31]; we will not consider it further here.

If the degree of polarization of the field is unity and its state of polarization is uniform, e.g., if the field is linearly polarized or left-circularly polarized everywhere, then the field and its correlation function may be treated as scalar quantities. The correlation properties of such a scalar wave field,  $U(\mathbf{r}, \omega)$ , are characterized by the cross-spectral density function [30]

$$W(\mathbf{r}_1, \mathbf{r}_2, \omega) = \langle U^*(\mathbf{r}_1, \omega) U(\mathbf{r}_2, \omega) \rangle, \quad (8)$$

and its normalized version, the spectral degree of coherence

$$\mu(\mathbf{r}_1, \mathbf{r}_2, \omega) = \frac{\langle U^*(\mathbf{r}_1, \omega) U(\mathbf{r}_2, \omega) \rangle}{\sqrt{S(\mathbf{r}_1, \omega) S(\mathbf{r}_2, \omega)}}, \quad (9)$$

with the spectral density  $S(\mathbf{r}, \omega)$  defined as

$$S(\mathbf{r}, \omega) = W(\mathbf{r}, \mathbf{r}, \omega). \quad (10)$$

At each position  $\mathbf{r}$  the cross-spectral density matrix (2) can be decomposed in a unique manner into two parts, viz.  $\mathbf{W}^{(p)}(\mathbf{r}, \mathbf{r}, \omega)$ , which represents the fully polarized part of the field, and  $\mathbf{W}^{(u)}(\mathbf{r}, \mathbf{r}, \omega)$ , which represents the completely unpolarized part of the field [20, 32], i.e.,

$$\mathbf{W}(\mathbf{r}, \mathbf{r}, \omega) = \mathbf{W}^{(p)}(\mathbf{r}, \mathbf{r}, \omega) + \mathbf{W}^{(u)}(\mathbf{r}, \mathbf{r}, \omega). \quad (11)$$

These two parts have the form

$$\mathbf{W}^{(p)}(\mathbf{r}, \mathbf{r}, \omega) = \begin{bmatrix} B(\mathbf{r}, \mathbf{r}, \omega) & D(\mathbf{r}, \mathbf{r}, \omega) \\ D^*(\mathbf{r}, \mathbf{r}, \omega) & C(\mathbf{r}, \mathbf{r}, \omega) \end{bmatrix}, \quad (12)$$

$$\mathbf{W}^{(u)}(\mathbf{r}, \mathbf{r}, \omega) = \begin{bmatrix} A(\mathbf{r}, \mathbf{r}, \omega) & 0 \\ 0 & A(\mathbf{r}, \mathbf{r}, \omega) \end{bmatrix}, \quad (13)$$

with  $A, B, C \geq 0$ ,  $D \in \mathbb{C}$ , and

$$BC - DD^* = 0. \quad (14)$$

These four quantities can be expressed in terms of the elements of  $\mathbf{W}(\mathbf{r}, \mathbf{r}, \omega)$  as

$$A(\mathbf{r}, \mathbf{r}, \omega) = \frac{1}{2} \left[ W_{xx} + W_{yy} - \sqrt{(W_{xx} - W_{yy})^2 + 4|W_{xy}|^2} \right], \quad (15)$$

$$B(\mathbf{r}, \mathbf{r}, \omega) = \frac{1}{2} \left[ W_{xx} - W_{yy} + \sqrt{(W_{xx} - W_{yy})^2 + 4|W_{xy}|^2} \right], \quad (16)$$

$$C(\mathbf{r}, \mathbf{r}, \omega) = \frac{1}{2} \left[ W_{yy} - W_{xx} + \sqrt{(W_{xx} - W_{yy})^2 + 4|W_{xy}|^2} \right], \quad (17)$$

$$D(\mathbf{r}, \mathbf{r}, \omega) = W_{xy}. \quad (18)$$

We note that this decomposition applies locally at each point, but that an electromagnetic wave cannot be generally decomposed into an unpolarized wave and a fully polarized wave, see [33]. The spectral Stokes parameters pertaining to the fully polarized part of the field are defined as [30]

$$S_0(\mathbf{r}, \omega) = B + C = \sqrt{(W_{xx} - W_{yy})^2 + 4|W_{xy}|^2}, \quad (19)$$

$$S_1(\mathbf{r}, \omega) = B - C = W_{xx} - W_{yy}, \quad (20)$$

$$S_2(\mathbf{r}, \omega) = D + D^* = W_{xy} + W_{yx}, \quad (21)$$

$$S_3(\mathbf{r}, \omega) = i(D^* - D) = i(W_{yx} - W_{xy}). \quad (22)$$

The angle  $\psi$  between the major axis of the polarization ellipse and the positive  $x$  axis is given by the expression [20]

$$\psi = \frac{1}{2} \arctan \left( \frac{S_2}{S_1} \right), \quad (0 \leq \psi < \pi). \quad (23)$$

In the remainder we will use the normalized version of the Stokes parameters by defining

$$s_i(\mathbf{r}, \omega) \equiv S_i(\mathbf{r}, \omega)/S_0(\mathbf{r}, \omega), \quad (i = 1, 2, 3). \quad (24)$$

Two types of polarization singularities can be identified. At C points, points where  $s_3(\mathbf{r}, \omega) = \pm 1$ , the polarization is left circular or right circular. This means that the orientation angle  $\psi$  is undefined. At L lines, there where  $s_3(\mathbf{r}, \omega) = 0$ , the polarization is linear. At such lines the handedness of the polarization ellipse is undefined. Just as phase singularities possess a conserved topological charge, C points possess a conserved topological index. For a given wave field feature, the topological index may be defined as the number of rotations that the polarization ellipse undergoes as one traverses a closed path around the feature in a counter-clockwise manner. Because the polarization field is continuous everywhere on the path, the ellipse must return to its original orientation in one full circuit; however, because the ellipse is symmetric under  $180^\circ$  rotations, the minimum topological index is  $\pm 1/2$ . The polarization ellipses in the vicinity of a C point can take on one of three generic forms. Their major axis can form a star, a lemon or a monstar pattern [4]. A star has index  $-1/2$ , whereas a lemon and a monstar both have index  $+1/2$ . Under smooth transformations of the system parameters, both topological charge and index are conserved quantities.

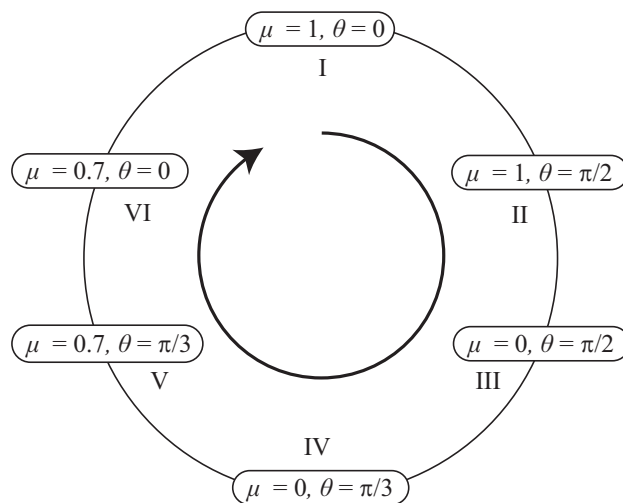


Fig. 1. Illustrating the continuous cycle in which the coherence parameter  $\mu$  and the polarization angle  $\theta$  are smoothly varied, and eventually brought back to their initial values. Stage I is at the top of the figure.

In the next section we describe a three-pinhole interferometer in which all these different types of singularities can be created by altering the state of polarization and coherence of the incident beam in a cyclical manner. This is achieved by varying the polarization angle  $\theta$  at the first pinhole, and the coherence parameter  $\mu$ . The precise definition of the latter is given in the next section. The various stages of the cycle are depicted in Fig. 1.

### 3. Young's experiment with three pinholes

We consider an opaque screen with three identical pinholes that lie on the vertices of an equilateral triangle (see Fig. 2). The screen is located in the plane  $z = 0$ , and is illuminated by a normally incident electromagnetic beam of frequency  $\omega$ . An interference pattern is formed on a second, parallel screen at a distance  $\Delta z$ . The two-dimensional position vectors of the pinholes

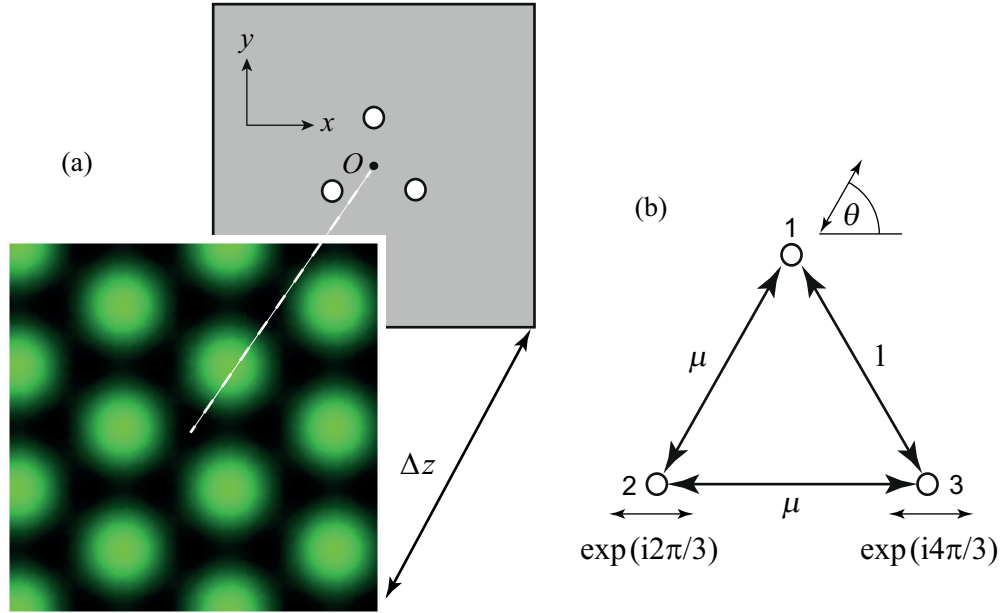


Fig. 2. Three identical pinholes in an opaque screen occupying the plane  $z = 0$ . The pinholes are located symmetrically with respect to the origin  $O$  of a right-handed Cartesian coordinate system. An interference pattern is formed on a second, parallel screen a distance  $\Delta z$  away (a). The three pinholes with their relative phase, coherence parameter, and orientation of the electric field (b).

are

$$\rho_1 = \rho(0, 1), \quad (25)$$

$$\rho_2 = \rho(-\sqrt{3}/2, -0.5), \quad (26)$$

$$\rho_3 = \rho(\sqrt{3}/2, -0.5), \quad (27)$$

respectively. Assuming that the angles of diffraction are small, the electric field at a position  $\mathbf{r}$  on the observation screen is given by the sum of the three pinhole contributions, i.e.

$$\mathbf{E}(\mathbf{r}, \omega) = \sum_{i=1}^3 K_i(\mathbf{r}, \omega) \mathbf{E}(\rho_i, \omega), \quad (28)$$

where  $K_i(\mathbf{r}, \omega)$  is a propagator, given by the expression [20, Sec. 8.3]

$$K_i(\mathbf{r}, \omega) = -\frac{i}{\lambda} \frac{e^{ikR_i}}{R_i} dA, \quad (i = 1, 2, 3), \quad (29)$$

with  $\lambda$  the free-space wavelength, and  $k$  the wavenumber associated with frequency  $\omega$ . Furthermore,  $dA$  denotes the area of each pinhole, and  $R_i$  is the distance from pinhole  $i$  to the observation point  $\mathbf{r}$ . The two-dimensional vectors  $\mathbf{E}(\rho_i, \omega)$  denote the transverse electric field incident at the three pinholes.

#### 4. Transformation of singularities

##### Stage I: Phase singularities

The incident fields at the pinholes,  $\mathbf{E}(\rho_i, \omega)$  with  $i = 1, 2, 3$ , are first taken to be fully coherent ( $\mu = 1$ ). Both  $\mathbf{E}(\rho_2, \omega)$  and  $\mathbf{E}(\rho_3, \omega)$  are linearly polarized along the  $x$  direction. The field  $\mathbf{E}(\rho_1, \omega)$  however, has a polarization which makes a variable angle  $\theta$  with the  $x$  axis, see Fig. 2. The relative phase differences of the three fields are set such that

$$\mathbf{E}(\rho_1, \omega) = C(\cos \theta \hat{\mathbf{x}} + \sin \theta \hat{\mathbf{y}}), \quad (30)$$

$$\mathbf{E}(\rho_2, \omega) = C e^{i2\pi/3} \hat{\mathbf{x}}, \quad (31)$$

$$\mathbf{E}(\rho_3, \omega) = C e^{i4\pi/3} \hat{\mathbf{x}}, \quad (32)$$

with  $C$  an arbitrary complex-valued amplitude, and  $\hat{\mathbf{x}}$  and  $\hat{\mathbf{y}}$  unit vectors along the  $x$  and  $y$  axis. A time-dependent factor  $\exp(-i\omega t)$  is suppressed. As we will discuss shortly, the phase differences are chosen such that a phase singularity centered on the  $z$  axis is produced. To simplify the notation, we from now on no longer display the  $\omega$  dependence of the various quantities.

Initially the polarization angle of the field at pinhole 1 is set to zero, i.e., we start the cycle at the top of Fig. 1 with  $\mu = 1$  and  $\theta = 0$ .

The spectral density distribution on the observation screen then has a hexagonal shape, as can be seen from Fig. 3(a). For a point on the central  $z$  axis the three propagators  $K_i(\mathbf{r})$  appearing in Eq. (28) all have the same value, and hence it readily follows that now

$$E_x(0, 0, z) = 0. \quad (33)$$

In other words, the electric field component  $E_x$  has a phase singularity at position  $(x, y, z) = (0, 0, \Delta z)$ . It is seen from Fig. 3(b), in which the phase of  $E_x$  is plotted, that this singularity has topological charge  $s = 1$ . Other phase singularities, some with  $s = 1$ , others with  $s = -1$ , are visible as well. Although the sharp boundaries between different colors might suggest otherwise, we note that the phase changes continuously everywhere, with the exception of the singular points.

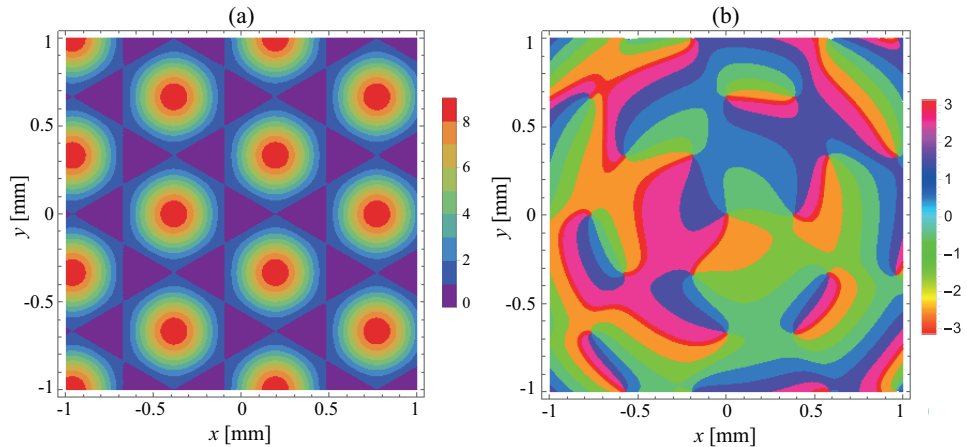


Fig. 3. The spectral density  $S(x, y) = |\mathbf{E}(x, y)|^2$  in arbitrary units (a), and the color-coded phase of  $E_x(x, y)$  on the observation screen (b). In this example the polarization angle  $\theta = 0$ ,  $\mu = 1$ ,  $\lambda = 0.5 \times 10^{-6}$  m,  $\rho = 0.5$  mm, and  $\Delta z = 1$  m.



For completeness' sake we note that the  $z$  axis also represents a singularity of the Poynting vector [34]. Because the field everywhere is linearly polarized, no C points exist at stage I.

*Stage II: Polarization singularities and coherence singularities in fully coherent fields*

Next  $\theta$ , the angle of polarization of the electric field at pinhole 1, is gradually increased from 0 to  $\pi/2$ . Since this breaks the symmetry of the system, we expect the central phase singularity on the  $z$  axis to decay into a pair of polarization singularities, namely two C points of opposite handedness, and with opposite index, which are separated by an L line. This is because when we describe the field in terms of the left and right-circular polarization basis ( $\epsilon_+$ ,  $\epsilon_-$ ) [35], this phase singularity of  $E_x$  is a zero of both  $\epsilon_+$  and  $\epsilon_-$ . Increasing  $\theta$  perturbs the highly symmetric field distribution on the observation screen, and the zeros of  $\epsilon_+$  and  $\epsilon_-$  will no longer coincide. This means that two C points, with opposite handedness, have been created. Conservation of index implies that one singularity has index  $1/2$  whereas the other has an index  $-1/2$ . This is illustrated by Fig. 4(a) in which the orientation of the major axis of the polarization ellipse is plotted in the region around the  $z$  axis. Two polarization singularities can be seen. Tracking the change of the orientation of the major polarization axis around these features shows that the upper one is a lemon with index  $1/2$ , whereas the lower one is a star with index  $-1/2$ . A plot of the contours of the Stokes parameters, Fig. 4(b), shows that the lemon has  $s_3 = 1$ , i.e. it is a point of right circular polarization (a zero of  $\epsilon_-$ ), whereas the star has  $s_3 = -1$ , indicating it is a point of left circular polarization (a zero of  $\epsilon_+$ ). Because the Stokes parameters on the Poincaré sphere are continuous functions of the point of observation [36], we expect that the two C points are separated by a region of linear polarization, i.e. an L line at which  $s_3(x, y) = 0$ . This is indeed the case as is evidenced by the orange contour line. The same creation of a pair of C points separated by an L line is also found to happen at the other phase singularities of Fig. 3(b) when the angle  $\theta$  is increased from zero. The pairs move away from each other and remain extant as  $\theta$  reaches its maximum value of  $\pi/2$ .

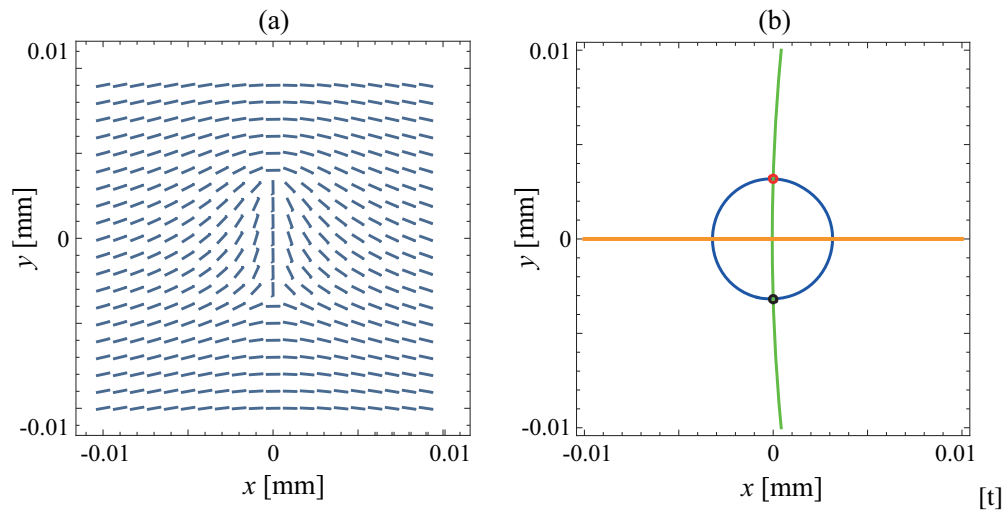


Fig. 4. The local orientation of the major axis of the polarization ellipse after the angle of polarization at pinhole 1 has been increased from zero to  $\theta = 0.03$ . The phase singularity of  $E_x$  at  $(0, 0)$  in Fig. 3 has decayed into two polarization singularities: a lemon (top) and a star (bottom) (a). Selected contours of the Stokes parameters for the same region as in the left-hand panel:  $s_1 = 0$  (blue),  $s_2 = 0$  (green),  $s_3 = 0.998$  (red),  $s_3 = -0.998$  (black) and  $s_3 = 0$  (orange) (b). All other parameters are the same as in Fig. 3.

Changing the polarization angle  $\theta$  of the field at pinhole 1 also changes the electromagnetic spectral degree of coherence as defined by Eq. (5). For fully coherent fields, as studied at this stage of the cycle, it reduces to the form of Eq. (6). We take both  $\mathbf{r}_1$  and  $\mathbf{r}_2$  to be on the observation screen (i.e.,  $z_1 = z_2 = \Delta z$ ), and from now on suppress the  $z$  dependence in our notation. If we start out with  $\theta = 0$ , then for any choice of the reference point  $(x_1, y_1)$ , the electromagnetic spectral degree of coherence will be singular if  $(x_2, y_2)$  is taken as one of the phase singularities of  $E_x$  shown in Fig. 3(b). Let us choose a fixed reference point  $(x_1, y_1) = (0.45, 0)$  mm. In Fig. 5 we plot the phase of  $\eta(x_1, y_1, x_2, y_2)$  for selected values of the angle  $\theta$ . It is seen in panel (a) that the phase singularity of  $E_x$  at  $(0, 0)$  is indeed also a singular point of the electromagnetic spectral degree of coherence (with topological charge  $s = 1$ ). In other words, the two points  $(0.45, 0)$  mm and  $(0, 0)$  on the observation screen form an electromagnetic coherence singularity. Apart from the singularity on the  $z$  axis, other coherence singularities can be seen as well. On increasing the angle  $\theta$ , pairs of singularities with opposite topological charge are moving closer to one another (b). Around  $\theta = 0.77$  these pairs all annihilate, resulting in a singularity-free field as shown in panel (c). On further increasing the polarization angle to its maximum value of  $\pi/2$  the phase contours of  $\eta(x_1, y_1, x_2, y_2)$  change somewhat, but no new singularities are created (d). We note that the behavior of the electromagnetic degree of coherence is quite sensitive to the choice of the reference point  $\mathbf{r}_1$ . In summary, at Stage II we have C points, but no coherence singularities. Animations of the evolution of the phase of  $\eta(x_1, y_1, x_2, y_2)$  and the major polarization axes are given in [Visualization 1](#) and [Visualization 2](#), respectively.

### *Stage III: Coherence singularities and polarization singularities in partially coherent fields*

The singularities of the spectral degree of coherence that we have encountered so far occur in fully coherent fields. We next make the field partially coherent by randomizing  $\mathbf{E}(\rho_2)$  while keeping its polarization along the  $x$  axis.  $\mathbf{E}(\rho_1)$  and  $\mathbf{E}(\rho_3)$  remain fully correlated. We consider the case for which the first element of the cross-spectral density matrix  $\mathbf{W}(\rho_2, \rho_3)$  equals

$$W_{xx}(\rho_2, \rho_3) = |C|^2 \mu e^{i2\pi/3}, \quad (34)$$

with  $\mu$  real-valued and  $0 \leq \mu \leq 1$  (see Fig. 2(b)). The upper bound corresponds to full coherence, the lower bound corresponds to a complete absence of coherence. For all intermediate values the fields are said to be partially coherent. The scalar coherence parameter  $\mu$  is designed to be the magnitude of the degree of coherence between the pinholes. From Eq. (34) all other matrix elements can be derived, and from them the electromagnetic degree of coherence, as given by Eq. (5), can then be calculated. This is described in Appendix A.

We change the field from fully coherent to partially coherent by gradually decreasing  $\mu$ . We start at the situation depicted in panel (d) of Fig. 5, i.e., the reference point  $(x_1, y_1) = (0.45, 0)$  mm, and the polarization angle  $\theta = \pi/2$ . First  $\mu = 1$ , meaning that the fields at the three pinholes are fully coherent. The phase contours of the spectral degree of coherence  $\eta(x_1, y_1, x_2, y_2)$  for that situation are reproduced in Fig. 6(a). If  $\mu$  is gradually decreased we see the birth of partially coherent electromagnetic correlation vortices near  $\mu = 0.57$ , see panel (b). On further decreasing  $\mu$  pairs of singularities of opposite charge move away from each other, as shown in panel c. No further topological reactions are observed as  $\mu$  reaches its lowest value 0, which corresponds with the situation shown in panel (d).

As the coherence parameter  $\mu$  is decreased from unity, the polarized portion of the field initially displays both C points and L lines, however, near  $\mu = 0.5$  pairs of C points annihilate each other. But these events are not the inverse of the creation process that was presented in Fig. 4 of stage II. There the pairs of C points had opposite handedness because they were created from a decaying phase singularity. Here C points with equal handedness (i.e., with the same value of  $s_3$ ) annihilate, which does therefore not result in the creation of a phase

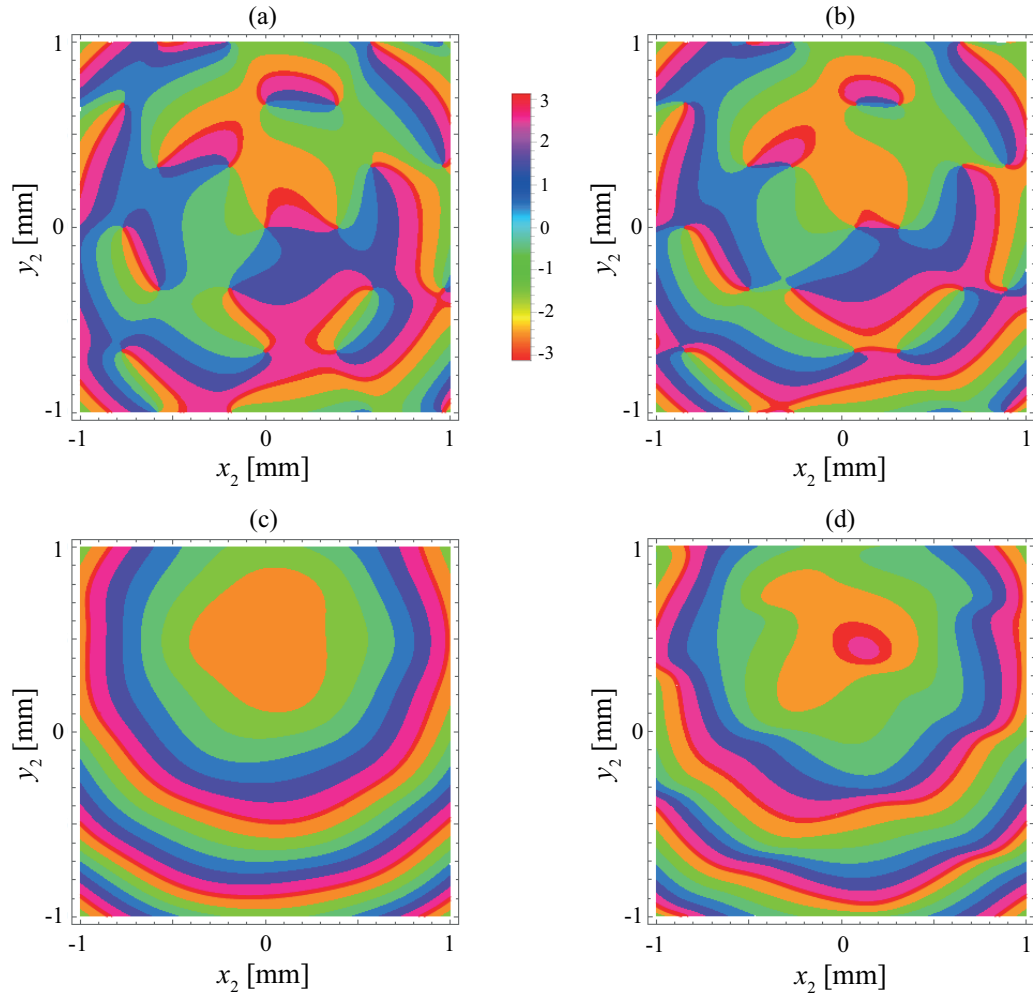


Fig. 5. Color-coded plot of the phase of the spectral degree of coherence  $\eta(x_1, y_1, x_2, y_2)$  on the observation screen. The reference point is taken as  $(x_1, y_1) = (0.45, 0)$  mm. The polarization angle  $\theta = 0$  (a), 0.65 (b), 1.12 (c), and  $\pi/2$  (d). All other parameters are the same as in Fig. 3.

singularity of the polarized part of the field. This annihilation process in which two vertical contours of  $s_1 = 0$  (blue) coalesce and disappear is illustrated in Fig. 7(a). After this event the contours of  $s_2 = 0$  (green) and the L lines (orange), remain in existence, as shown in panel (b). We conclude that at Stage III, we have no C points, but coherence singularities are present. Animations of the evolution of the phase of  $\eta(x_1, y_1, x_2, y_2)$  and the major polarization axes are given in [Visualization 3](#) and [Visualization 4](#), respectively.

#### Stage IV: Polarization ellipse fields

If we now rotate the polarization angle  $\theta$  partly back from  $\pi/2$  to  $\pi/3$ , while keeping  $\mu$  fixed at 0, no topological reactions are observed. However, the polarization ellipses pertaining to the polarized portion of the field slightly change their shape and orientation. The coherence singularities remain during this parameter change (not shown). So, at Stage IV there are no C points but coherence singularities exist. Animations of the evolution of the phase of  $\eta(x_1, y_1, x_2, y_2)$

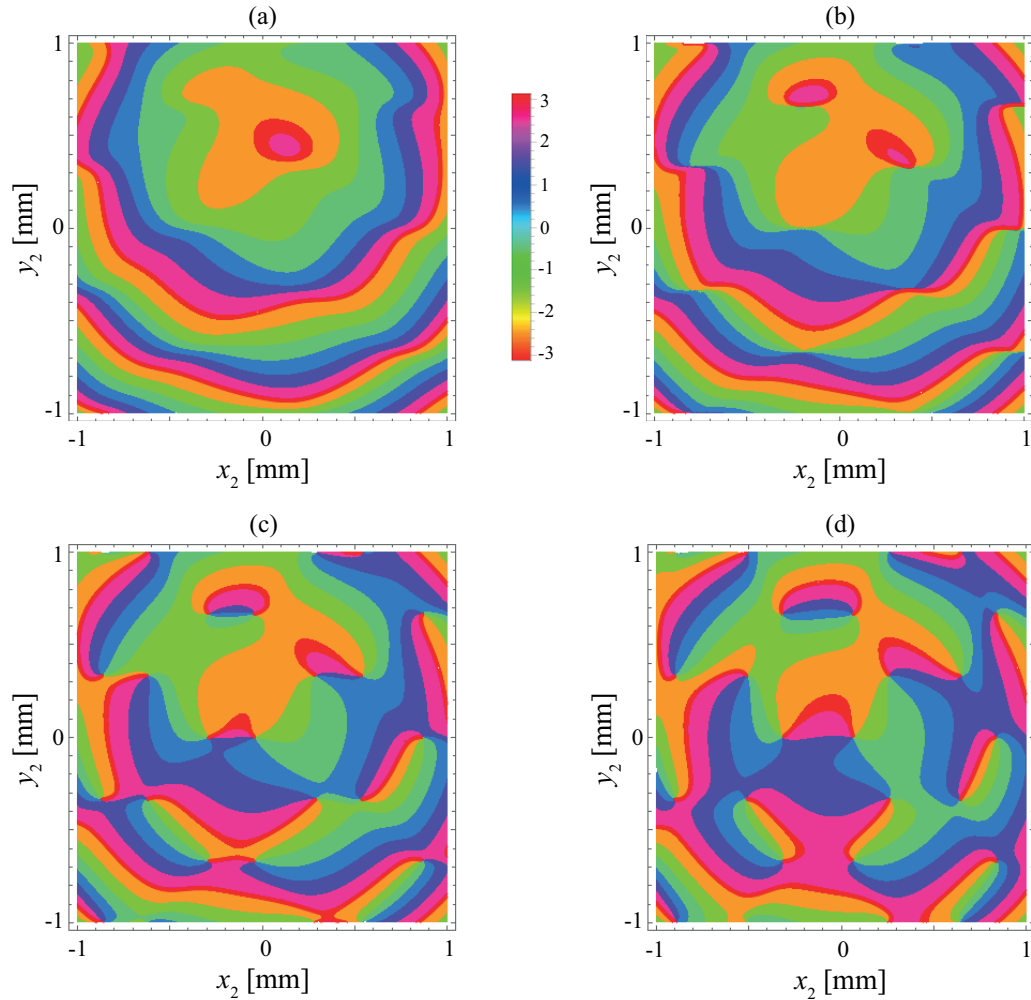


Fig. 6. Color-coded plot of the phase of the spectral degree of coherence  $\eta(x_1, y_1, x_2, y_2)$  on the observation screen. The reference point is taken as  $(x_1, y_1) = (0.45, 0)$  mm. The polarization angle  $\theta = \pi/2$ . The coherence parameter  $\mu = 1$  (a), 0.57 (b), 0.40 (c), and 0 (d). All other parameters are the same as in Fig. 3.

and the polarization major axes are given in [Visualization 5](#) and [Visualization 6](#), respectively.

#### Stage V: Creation of polarization singularities

In this stage we keep the angle  $\theta$  fixed at  $\pi/3$ , and gradually increase the coherence parameter  $\mu$  to 0.7. This first changes the orientation of the polarization ellipses. In Fig. 8(a) the major axis of these ellipses are shown for the case  $\mu = 0.4$ . Near  $\mu = 0.5$  pairs of polarization singularities, namely C points with opposite handedness separated by an L line, are created. For larger values of  $\mu$  these singular points move away from each other. They can be clearly seen in Fig. 8(b). The nature of these singularities can be deduced from analyzing contours of the Stokes parameters. These are presented in Fig. 9. The blue and green curves correspond to  $s_1 = 0$  and  $s_2 = 0$ , respectively. Their intersections are C points with either  $s_3 = 1$  (red) or  $s_3 = -1$  (black). L lines, the contours  $s_3 = 0$ , are plotted in orange. We see, for example, that the star singularity

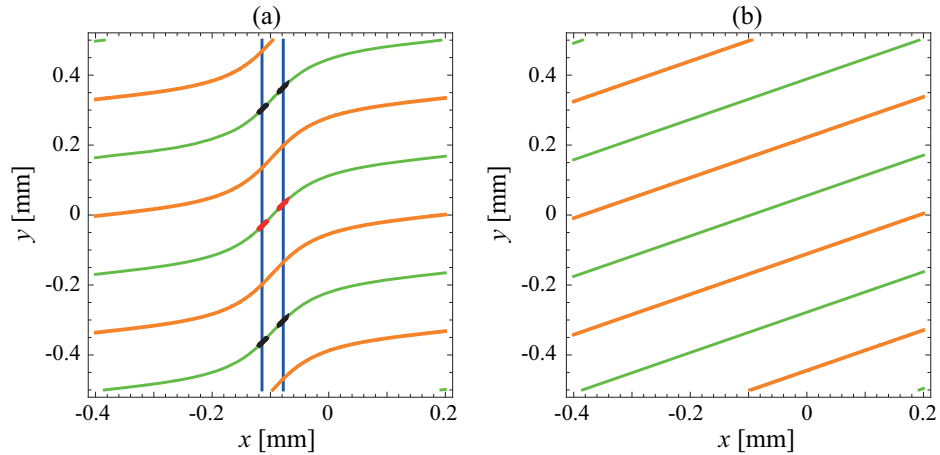


Fig. 7. Contours of the Stokes parameters for the case  $\mu = 0.51$  and  $\theta = \pi/2$ , just before the annihilation of pairs of C points with the same handedness (a). Shown are contours of  $s_3 = 0.9999$  (red),  $s_3 = -0.9999$  (black),  $s_1 = 0$  (blue),  $s_2 = 0$  (green), and  $s_3 = 0$  (orange). In (b) the situation for  $\mu = 0$  and  $\theta = \pi/2$  is plotted. All other parameters are the same as in Fig. 3.

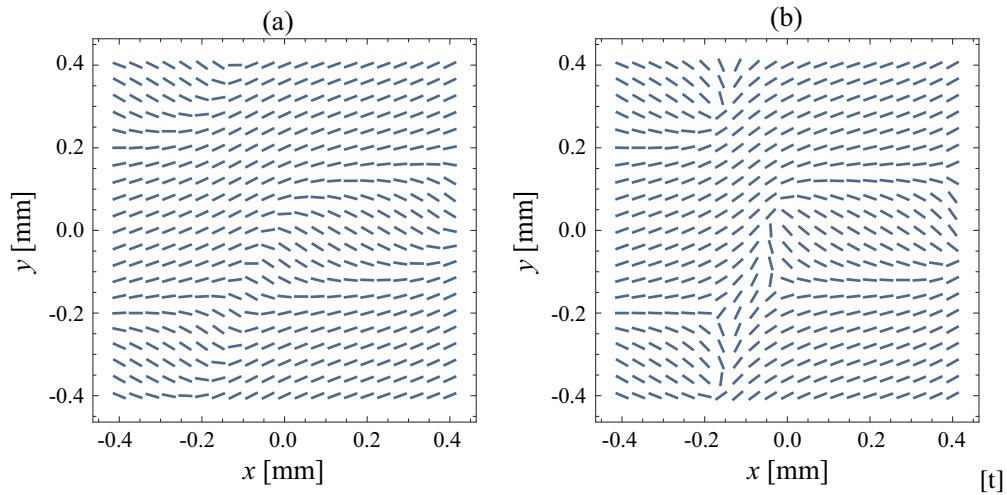


Fig. 8. Showing the major axis of the polarization ellipse field for two values of the coherence parameter  $\mu$  with the polarization angle  $\theta = \pi/3$ . In panel (a)  $\mu = 0.4$  and no C points are exist. In panel (b)  $\mu = 0.7$  and several C points have been created. All other parameters are the same as in Fig. 3.

near  $(x, y) = (-0.2, -0.2)$  mm has  $s_3 = 1$ , meaning that it is right-handed. It is separated by an L line from the left-handed lemon near  $(x, y) = (-0.2, -0.4)$  mm that has  $s_3 = -1$ . During this change of  $\mu$  the coherence singularities disappear (not shown). In summary, at Stage V we have polarization singularities, but no coherence singularities. Animations of the evolution of the phase of  $\eta(x_1, y_1, x_2, y_2)$  and the polarization major axes are given in [Visualization 7](#) and [Visualization 8](#), respectively.

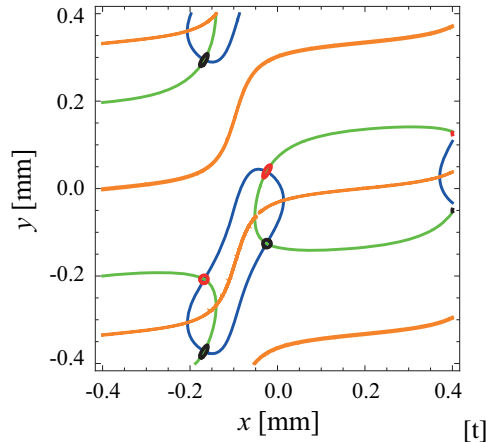


Fig. 9. Contour lines of the Stokes parameters corresponding to Fig. 8(b), i.e.,  $\theta = \pi/3$  and  $\mu = 0.7$ . The different contours represent  $s_1 = 0$  (blue),  $s_2 = 0$  (green),  $s_3 = 0.995$  (red),  $s_3 = -0.995$  (black), and  $s_3 = 0$  (orange). All other parameters are the same as in Fig. 3.

#### Stage VI: Annihilation of polarization singularities

We now keep the coherence parameter  $\mu$  fixed at 0.7 while the polarization angle  $\theta$  is gradually changed from  $\pi/3$  to 0. The C points that were created in the previous stage move back together as  $\theta$  decreases. This is illustrated in Fig. 10. In panel (a) Stokes contours for  $\theta = 0.9$  are plotted. Notice that the blue curve  $s_1 = 0$  self-intersects, which corresponds to a saddle point. Within the numerical accuracy, this saddle point lies on an orange curve  $s_3 = 0$ , which means that at this point  $s_2 = 1$ , i.e., the (polarized part of the) field there is linearly polarized under an angle of  $45^\circ$  with the  $x$  axis. If  $\theta$  is further decreased, the  $s_1 = 0$  contours break up into two closed curves that gradually contract until  $\theta = 0.8$ , at which point the curves cease to exist and two pairs of C points annihilate. The contours of  $s_2 = 0$  and  $s_3 = 0$  remain, as shown in panel b. At the points where the contours cross each other,  $s_1 = 1$ , which means that the field there is  $x$ -polarized. If the angle  $\theta$  reaches its original value of zero, the polarized portion of the field becomes, obviously, everywhere  $x$ -polarized. Therefore at Stage VI we find no C points, but correlation singularities are present (not shown). Because the polarization is uniform, these are, in fact, scalar correlation singularities. Animations of the evolution of the phase of  $\eta(x_1, y_1, x_2, y_2)$  and the polarization major axes are given in [Visualization 9](#) and [Visualization 10](#), respectively.

We can complete the cycle by increasing the coherence parameter  $\mu$  from 0.7 to unity, bringing the system back to Stage I. This means that the field changes from being partially coherent to fully coherent. [Visualization 11](#) shows the phase singularity evolution from stage VI to the initial Stage I.

## 5. Conclusions

We have demonstrated that it is possible to design a simple three-pinhole interferometer in which multiple types of singularities can be created and annihilated in a continuous, cyclical manner. A rich variety of transformations was observed. For instance, the breakup of a phase singularity into a pair of C points of opposite handedness is seen, along with the annihilation of pairs of C points with identical handedness which does not produce a phase singularity. The interrelations between phase, correlation and eta singularities are demonstrated, and it is seen by example that a decrease in coherence can in fact lead to a creation of eta singularities in some cases. For this particular system configuration, a striking anti-correlation between the presence

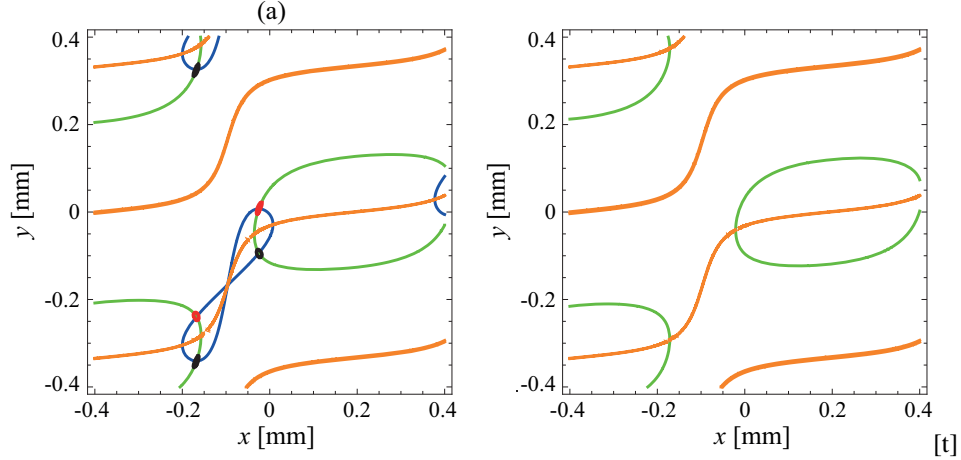


Fig. 10. Contour lines of the Stokes parameters when  $\mu = 0.7$  and  $\theta = 0.90$  (a) and  $\theta = 0.75$ . The different contours represent  $s_1 = 0$  (blue),  $s_2 = 0$  (green),  $s_3 = 0.995$  (red),  $s_3 = -0.995$  (black), and  $s_3 = 0$  (orange). All other parameters are the same as in Fig. 3.

of coherence singularities and the presence of C points was observed.

This interferometer represents a simple tool which can be used to study and/or generate various types of singularities simultaneously, but also the transitions between them.

## Appendix A

In this Appendix we present the derivation of the other relevant elements of the cross-spectral density matrices. Since, according to Eqs. (30) and (32),

$$E_x(\rho_1) = \cos \theta e^{-i4\pi/3} E_x(\rho_3), \quad (35)$$

it follows Eq. (34) that

$$W_{xx}(\rho_2, \rho_1) = \cos \theta e^{-i4\pi/3} W_{xx}(\rho_2, \rho_3), \quad (36)$$

$$= |C|^2 \mu \cos \theta e^{-i2\pi/3}. \quad (37)$$

Furthermore, because

$$E_y(\rho_1) = (\sin \theta / \cos \theta) E_x(\rho_1), \quad (38)$$

we find both that

$$W_{xy}(\rho_1, \rho_1) = |C|^2 \sin \theta \cos \theta, \quad (39)$$

$$W_{xy}(\rho_2, \rho_1) = (\sin \theta / \cos \theta) W_{xx}(\rho_2, \rho_1), \quad (40)$$

$$= |C|^2 \mu \sin \theta e^{-i2\pi/3}. \quad (41)$$

Similarly, we have from Eq. (35) that

$$E_x^*(\rho_1) = \cos \theta e^{i4\pi/3} E_x^*(\rho_3). \quad (42)$$

This implies

$$W_{xx}(\rho_1, \rho_3) = \cos \theta e^{i4\pi/3} W_{xx}(\rho_3, \rho_3), \quad (43)$$

$$= |C|^2 \cos \theta e^{i4\pi/3}. \quad (44)$$

Finally, Eq. (38) also gives

$$W_{yx}(\rho_1, \rho_3) = (\sin \theta / \cos \theta) W_{xx}(\rho_1, \rho_3), \quad (45)$$

$$= |C|^2 \sin \theta e^{i4\pi/3}. \quad (46)$$

All other elements of the three cross-spectral density matrices  $\mathbf{W}(\rho_2, \rho_1)$ ,  $\mathbf{W}(\rho_1, \rho_3)$  and  $\mathbf{W}(\rho_2, \rho_3)$  are zero. It immediately follows from Eqs. (30)–(32) that the spectral densities associated with the  $x$  and  $y$  components of the field at the three pinholes, which are given by the “diagonal” matrix elements, equal

$$S_x(\rho_1) = W_{xx}(\rho_1, \rho_1) = |C|^2 \cos^2 \theta, \quad (47)$$

$$S_y(\rho_1) = W_{yy}(\rho_1, \rho_1) = |C|^2 \sin^2 \theta, \quad (48)$$

$$S_x(\rho_2) = W_{xx}(\rho_2, \rho_2) = |C|^2, \quad (49)$$

$$S_x(\rho_3) = W_{xx}(\rho_3, \rho_3) = |C|^2. \quad (50)$$

On making use of Eq. (28) and the above expressions for the cross-spectral density matrices we find that the spectral density at a point  $(x, y)$  on the observation screen equals

$$S(x, y) = \langle |E_x(x, y)|^2 \rangle + \langle |E_y(x, y)|^2 \rangle, \quad (51)$$

$$= |C|^2 \left[ |K_1(x, y)|^2 + |K_2(x, y)|^2 + |K_3(x, y)|^2 + 2\mu \cos \theta \operatorname{Re} \left\{ K_2^*(x, y) K_1(x, y) e^{-i2\pi/3} \right\} \right. \\ \left. + 2 \cos \theta \operatorname{Re} \left\{ K_1^*(x, y) K_3(x, y) e^{i4\pi/3} \right\} + 2\mu \operatorname{Re} \left\{ K_2^*(x, y) K_3(x, y) e^{i2\pi/3} \right\} \right]. \quad (52)$$

In a similar way it can be derived that

$$\operatorname{Tr} \mathbf{W}(x_1, y_1, x_2, y_2) = |C|^2 \left\{ K_1^*(x_1, y_1) K_1(x_2, y_2) + K_2^*(x_1, y_1) K_2(x_2, y_2) + K_3^*(x_1, y_1) K_3(x_2, y_2) \right. \\ \left. + \mu \cos \theta \left[ K_1^*(x_1, y_1) K_2(x_2, y_2) e^{i2\pi/3} + K_2^*(x_1, y_1) K_1(x_2, y_2) e^{-i2\pi/3} \right] \right. \\ \left. + \cos \theta \left[ K_1^*(x_1, y_1) K_3(x_2, y_2) e^{i4\pi/3} + K_3^*(x_1, y_1) K_1(x_2, y_2) e^{-i4\pi/3} \right] \right. \\ \left. + \mu \left[ K_2^*(x_1, y_1) K_3(x_2, y_2) e^{i2\pi/3} + K_3^*(x_1, y_1) K_2(x_2, y_2) e^{-i2\pi/3} \right] \right\}. \quad (53)$$

The above two expressions allow us to calculate the evolution of the spectral degree of coherence  $\eta(x_1, y_1, x_2, y_2)$ , as given by Eq. (5), as the angle  $\theta$  and/or the coherence parameter  $\mu$  is being changed.

## Acknowledgments

G. Gbur’s research is supported by the U.S. Air Force Office of Scientific Research (USAFOSR) under Grant FA9550-13-1-0009. X. Pang and T. D. Visser’s work is supported by the Fundamental Research Funds for the Central Universities (grant No. 3102015ZY044), and the National Natural Science Foundations of China (NSFC) (grant No. 11504296).